ARTICLE

First-Principles Study of Field Emission from Zigzag Graphene Nanoribbons Terminated with Ether Groups

Xin Chen[a], Bin Li[b,c*]

a. Department of Physics, University of Science and Technology of China, Hefei 230026, China
b. Hefei National Laboratory for Physical Sciences at the Microscale, University of Science and Technology of China, Hefei 230026, China
c. Synergetic Innovation Center of Quantum Information & Quantum Physics, University of Science and Technology of China, Hefei 230026, China

(Dated: Received on May 1, 2015; Accepted on May 14, 2015)

Field emission properties of zigzag graphene nanoribbons terminated with C-O-C ether groups (including cyclic and alternative ether groups at edge, denoted as ZGNR-CE and ZGNR-AE) are studied by adopting a self-consistent method based on density functional theory calculation. The results show that the field emissions of these two nanoribbons are dominated by states around Brillouin zone center and close to Fermi level. Because of lower work function, the ZGNR-CE can produce much stronger emission current than reconstructed zigzag graphene nanoribbon. The ZGNR-AE has nearly completely spin-polarized emission current, although its emission current is not strong enough. It is also found that under the lower E-field, the uniaxial strain can effectively modulate their emission currents but the spin polarization of ZGNR-AE keeps unchanged with the varied strain. The underlying mechanisms are revealed by combining the analyses of their work functions and band structures with edge dipole model.

Key words: Field emission, Nanoribbon, Ether group, Density functional theory

I. INTRODUCTION

Among various applications for graphitic nanostructures, such as carbon nanotubes, graphene ribbons, field emission devices have raised high expectations for their notable advantages over traditional tip materials such as tungsten and molybdenum [1]. For example, carbon nanotube coated surface provides stable emission current and long lifetime which is related to its high aspect ratio and tight covalent bonds [2, 3]. Not only evaluation of work function but also examination of local electronic properties are important to understand mechanisms of field emission properties of the graphitic nanostructures [3]. Strictly, traditional Fowler-Nordheim (FN) formula [4, 5] applies only to field emission from bulk metals, so several methods have been introduced to study the field emission process of nanostructures [6–8]. For example, a scattering formalism based on the Lippmann-Schwinger (LS) equations was used to simulate the electron emission from various nanotubes, and localized states were found to be mainly responsible for the high current observed in open-ended nanotubes [6].

As low-dimensional carbon nanomaterial, graphene nanoribbons (GNR) have been investigated by numerous theoretical and experimental studies due to their exciting electronic, magnetic and spin filter properties [9]. Tada *et al.* first investigated the field emission properties of GNRs using the time-dependent density functional theory [8]. Details of this issue were probed into and clarified within the local density approximation (LDA) framework combined with wavefuntion matching method, and it was found that competition of many factors including band structure effect and wave function symmetry leads to specific energy distribution and intensity of the emission current [10]. Among the GNRs, the zigzag GNRs (ZGNR) intrigues great interests owing to its special electronic structure. Chemical modifications have been employed to modulate the field emission properties of ZGNR. For example, nitrogen doping has always been thought to be useful to enhance the electron field emission of graphene-like materials including the ZGNR [11–15]. Recently, the ZGNR terminated with cyclic ether groups also arouses interests of researchers because of its superior field emission properties shown by experiment [16], and reduction of the work function due to the cyclic C-O-C ether groups was suggested to result in enhancement of the electron emission [16, 17]. However, field emission simulation based on the first-principles and related analyses are still necessary to reveal role of the specific electronic state of

*Author to whom correspondence should be addressed. E-mail: libin@mail.ustc.edu.cn, Tel.: +86-551-63601747, FAX: +86-551-63601747

 ©2015 Chinese Physical Society

this nano-system in the field emission and further explore possible modulation of the emission properties.

In this work, we employ the approach combining density functional theory (DFT) calculation and wavefunction matching method [10, 18] to simulate the field emissions of two types of ZGNR terminated with C-O-C ether groups including cyclic and alternative ether groups at edge, denoted as ZGNR-CE and ZGNR-AE respectively. The ZGNR-CE can produce stronger field emission current which is dominated by the π-conjugated edge states, especially compared with reconstructed ZGNR [19]. The ZGNR-AE has ferromagnetic spin ordering at each edge so as to produce nearly completely spin-polarized emission current under appropriate electric field (E-field), but the current is not strong because of higher work function. We also explore possible modulations of their field emission properties by the uniaxial strain along the ribbon, and find that the appropriate compressive strain can significantly enhance the emission current of the ZGNR-CE under the lower E-field, but spin-polarization of the emission current of the ZGNR-AE is stable and not disturbed by the strain under the lower E-field. The work function and band structure along with the edge dipole model are combined to understand the above phenomena.

II. COMPUTATIONAL METHODS

The electronic structures of two ribbons under different E-fields are obtained by our first-principles calculations based on density functional theory (DFT) implemented the Vienna *ab initio* simulation package (VASP) [20–23]. Figure 1 shows structures of the ZGNR-CE and ZGNR-AE used for our simulation, along with that of the reconstructed ZGNR (ZGNR-RC) which is more stable than the unreconstructed one [19] and used here for comparison. A vacuum region of 15 Å between the ribbons (along x axis) is used, and in the z direction where the E-field is applied, the supercell has a vacuum thickness of 25 Å, which is necessary to perform the wave function matching when computing the emission current [10]. We adopt projector augmented wave (PAW) potentials [24] and generalized gradient approximation of Perdew, Burke, and Ernzerhof (GGA-PBE) [25], with a plane-wave cutoff of 520 eV. In order to sample k-points sufficiently in the two-dimensional (2D) Brillouin Zone (BZ) for the accurate calculation of the emission current [10], we use a **k** point mesh of 6×20×1 in the static calculations. All atoms are relaxed fully until forces become less than 0.02 eV/Å.

Our formulation for the field emission current is based on the DFT calculation and was ever described elsewhere [10]. The contribution from an eigenstate labled by (n, $\mathbf{k}_{//}$) to the emission current under an external

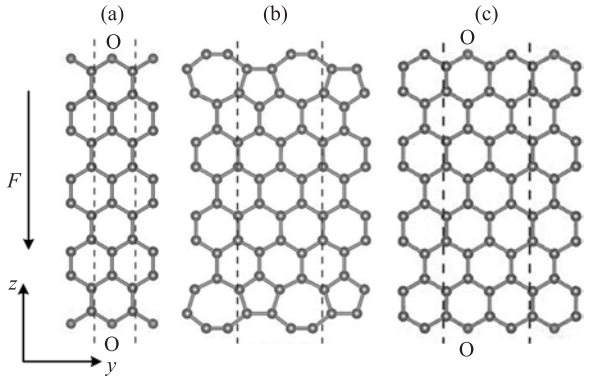

FIG. 1 Structural schematics of the unit cell for (a) the ZGNR-CE, (b) the ZGNR-RC, and (c) the ZGNR-AE. The boundaries of primitive cells along the z direction are shown using the dashed lines, and the E-field F is represented by an arrow. The O atoms are labeled and others are C atoms.

E-field F can be written as

$$J_{n,\mathbf{k}_{//}} = \sum_{\mathbf{G}_{//}} \frac{\hbar}{\pi m} \left(\frac{2meF}{\hbar^2}\right)^{1/3} |f_n(\mathbf{k}_{//}+\mathbf{G}_{//}, z_m)|^2 \cdot \left| Bi\left[\left(\frac{2meF}{\hbar^2}\right)^{1/3}(z_a - z_m)\right]\right|^{-2} \quad (1)$$

in which $f_n(\mathbf{k}_{//}+\mathbf{G}_{//}, z)$ is the plane-wave expansion coefficient of the eigenstate wavefunction, and $Bi\left[\left(\frac{2meF}{\hbar}\right)^{1/3}(z_a - z_m)\right]$ is Airy function. The total current energy distribution (TED) is

$$J(E) = 2\sum_{n,\mathbf{k}_{//}} \delta(E - \varepsilon_{n,\mathbf{k}_{//}})\eta(\varepsilon_{n,\mathbf{k}_{//}})J_{n,\mathbf{k}_{//}} \quad (2)$$

where $\eta(\varepsilon_{n,\mathbf{k}_{//}})$ is Fermi-Dirac occupation function. And total field emission current density is $J=\int J(E)\mathrm{d}E$. For the spin-polarized case, the spin-resolved field emission TED and total current densities ($J_{\mathrm{total},\alpha}$ and $J_{\mathrm{total},\beta}$) are computed using the spin-resolved eigenstates respectively, and electron spin polarization (ESP) of the emission current is defined as: $P=(J_{\mathrm{total},\alpha}-J_{\mathrm{total},\beta})/(J_{\mathrm{total},\alpha}+J_{\mathrm{total},\beta})$. The wavefunction matching point z_m is set to be 7 Å away from the ribbon edge, and the temperature related to $\eta(\varepsilon_{n,\mathbf{k}_{//}})$ is set to be 78 K. The qualitative results are nearly independent of the temperature.

III. RESULTS AND DISCUSSION

Figure 2(a) presents the TED curve of the field emission from the ZGNR-CE under a nominal E-field of 0.10 V/Å. The main peak is located near the Fermi

DOI:10.1063/1674-0068/28/cjcp1505087 ©2015 Chinese Physical Society

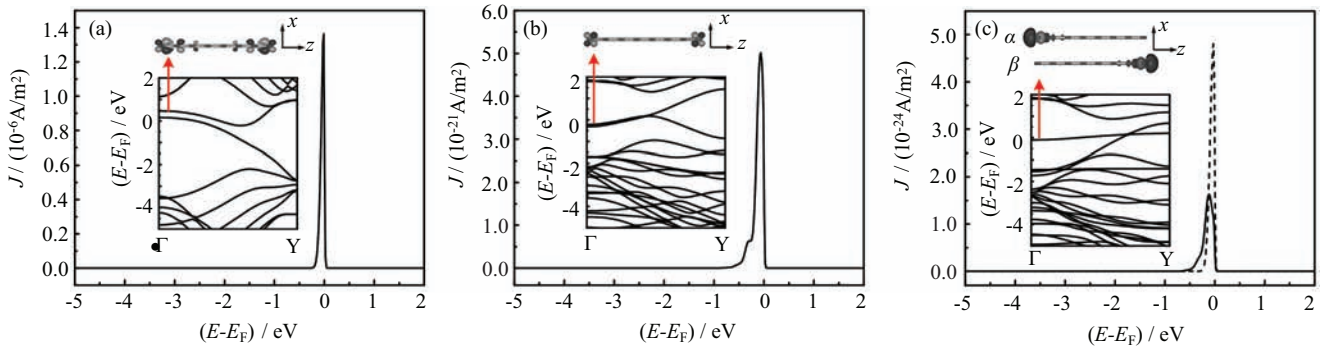

FIG. 2 TED curves of the field emission from three types of ribbons under the nominal E-field of 0.10 V/Å. (a) The ZGNR-CE, (b) the ZGNR-RC, and (c) the ZGNR-AE. In (c) the solid line represents the current with α spin which is magnified by 10^5 times, and the dash line represents the current with β spin. The insets give the band structures of three types of ribbons, and the wavefunction schematics of the Γ states indicated by the arrows are shown along with the structural model on the top of each figure respectively.

level (E_F). The result can be better understood in combination with its band structure, as shown by inset of Fig.2(a). This ribbon is metallic with two bands across the E_F, among which the band with obvious dispersion has Γ state in close proximity to the E_F. Wavefunction schematics of the Γ state of this band (on the top of Fig.2(a)) shows that it is an edge state mainly localized around the C-O-C ether groups and has π-conjugated characteristic. The states near (not including) the Γ point of this band should contribute tremendously to the emission current according to Eq.(1), because they have the highest eigen-energies among all the occupied states and smaller $\mathbf{k}_{//}$ so as to bring smaller z_a values, with non-zero $f_n(\mathbf{k}_{//}+\mathbf{G}_{//}, z)$ at the same time [10]. Similar situation occurs for the case of the ZGNR-RC. Different from the non-magnetic ZGNR-CE and ZGNR-RC, the ZGNR-AE has a magnetic ground state with opposite spin (antiferromagnetic) orientation between ferromagnetically ordered states at two edges, similar to the ZGNR [26]. The magnetism is mainly from unsaturated σ-type orbitals (dangling bond states) of C atoms at the edges with magnetic moment of 0.324 μ_B. Accordingly, the field emission from the ZGNR-AE is nearly completely spin-polarized with ESP of −100%, as shown by the TED curve (Fig.2(c)). The emission currents with two spins are dominated respectively by the degenerate Γ states of band close to the E_F (see inset in Fig.2(c)), which have σ characteristics so that the band are nearly flat, and are localized the C atoms at two edges respectively (see wavefunction schematics on the top of Fig.2(c)). This explains why the emission current with α spin is much larger than that with β spin because the emission occurs at one edge.

FN analyses based on the FN formula are important in field emission studies. We can perform FN analyses by calculating the total field emission current density J_{total} under different E-field value F. In the traditional field emission experiments, work function of emitter surface can be deduced from linear relationship of FN plot. Figure 3 shows FN plots for three types of ribbons. Here the actual E-field value F is obtained by differentiating the linear xy-averaged potential profile in the vacuum away from the emission edge, and is likely to deviate from the setting E-field value in the VASP calculation, depending on dielectric property of the system. Under the lower E-field, the emission current of the ZGNR-CE is much stronger than that of the ZGNR-RC with differences being even beyond ten orders of magnitude, whereas the emission currents from the ZGNR-AE are weaker than those from ZGNR-RC. But the emission currents for three types of ribbons have smaller differ-

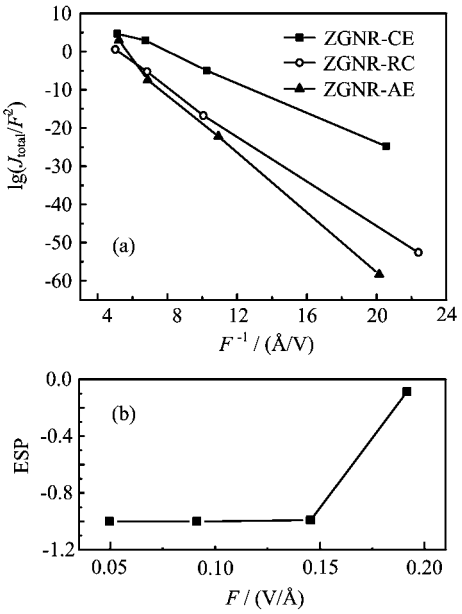

FIG. 3 (a) The FN plots of the field emissions from three types of ribbons. (b) The ESP of the emission current of the ZGNR-AE as a function of the actual E-field.

DOI:10.1063/1674-0068/28/cjcp1505087 ©2015 Chinese Physical Society

TABLE I The work functions of three types of ribbons: $\phi_{\rm FN}$ (deduced from the FN formula), $\phi_{\rm GGA}$ (calculated directly by the VASP using the GGA).

	$\phi_{\rm FN}$/eV	$\phi_{\rm GGA}$/eV
ZGNR-CE	3.55	3.56
ZGNR-RC	4.68	5.03
ZGNR-AE	5.52	5.33

ences and even of the same order of magnitude under the higher E-field. One can also see that the FN plots for the ZGNR-CE and ZGNR-AE can keep linear when the E-field is not larger than 0.15 V/Å, but their $J_{\rm total}$ values under the E-field of 0.2 V/Å deviate from this linear relationship a little.

Table I presents the work functions $\phi_{\rm FN}$ deduced from the FN formula (only fitting the points with lower E-fields)

$$J \propto F^2 \exp\left(-\frac{4\sqrt{2m}}{3\hbar e}\phi^{3/2}F^{-1}\right) \tag{3}$$

and the work functions $\phi_{\rm GGA}$ obtained directly by GGA calculations for three types of ribbons. The differences between the $\phi_{\rm FN}$ and $\phi_{\rm GGA}$ are small and mainly due to influence of image-potential [5] and that the states dominating the emission current are not perfectly at the $E_{\rm F}$ and Γ point [10]. On the other hand, there exist big differences between the work functions of three types of ribbons: the work function of ZGNR-CE is the lowest, and the one of ZGNR-AE is the highest. This work function difference determines that the ZGNR-CE has much stronger emission current than the other two ribbons under the lower E-field according to the FN formula Eq.(3). But the FN formula Eq.(3) also results in that increase of the emission current of the system having a lower work function with the enhanced E-field is slower than that having a higher work function. So the differences between the emission currents from three types of ribbons under the higher E-fields turn to be small. Our further examinations find that the higher external E-field brings great variations of the band structures near the $E_{\rm F}$, which are also responsible for these small differences. The ESP values of field emissions from the ZGNR-AE under different E-fields are also examined. The high spin-polarization of its emission current can keep under the lower E-field up to 0.15 V/Å, but under the E-field of 0.20 V/Å this spin-polarization is significantly weakened, which should be also ascribed to the great variations of the band structure near the $E_{\rm F}$ under the higher E-field.

The lower work function of the ZGNR-CE may be understood with help of edge dipole model [10]. The ZGNR-CE has positive edge dipole moment (pointing out), since the edge O atom has no dangling bond state so that the electrons are mainly localized between C and O atoms. According to formula of the work function in Wigner and Bardeen's theory [27]

$$\phi = -\mu - \frac{eP}{\varepsilon_0 A} \tag{4}$$

where μ is chemical potential in interior of the material, P and A are surface dipole moment and area per surface primitive cell respectively, the positive edge dipole moment results in the lower work function of the ZGNR-CE. However, for the ZGNR-AE, half of the edge atoms turn to the C atom with the dangling bond states as displayed before and then negative edge dipole moment, which nearly counteracts the role of the positive edge dipole moment from another half of edge atoms, *i.e.* O atoms, in decreasing the work function.

The work function is critical for the field emission properties according to the above analyses, and a lower work function can dramatically enhance the emission current. Recently Peng *et al.* found that work function of armchair graphene ribbon terminated with ether groups can be tuned by applying the external uniaxial strain [28]. Here our further investigations are concentrated on effect of the uniaxial strain on the field emission properties of the ZGNR-CE and ZGNR-AE. We apply the uniaxial strain along the ribbon within the range from -10% to 10% on the ZGNR-CE and ZGNR-AE. The negative value refers to compressive strain, while positive value corresponds to tensile strain. The calculated FN plots for two types of ribbons under different strain are presented in Fig.4. Similar to the cases without strain, the FN plots for various cases with different strains keep linear under the lower E-field but deviate a little under the higher E-field. For the ZGNR-CE (Fig.4(a)), under the lower E-field such as the nominal value 0.05 V/Å, the effect of the uniaxial strain on the emission current is more significant than that under the higher E-field. The inset in Fig.4(a) gives the total emission current density $J_{\rm total}$ as a function of the uniaxial strain under the nominal E-field of 0.05 V/Å. It is found that the $J_{\rm total}$ decreases monotonously with the tensile strain, but the relationship between the $J_{\rm total}$ and compressive strain is not monotonic and under the strain of about -5% the emission current reaches its maximum. For the ZGNR-AE (Fig.4(b)), the emission current differences between various cases with different strains are smaller even under the lower E-field than those of the ZGNR-CE. In this case the actual E-fields under different strains with the same nominal E-field have larger differences, which disturb our evaluation on the strain-dependence of the emission currents, so we use a dash vertical line at the E-field of 0.05 V/Å to indicate this dependence (Fig.4(b)). We have also examined the strain-dependence of the ESP of its emission current. Under the lower E-field such as the nominal value 0.05 V/Å, high spin-polarization of the emission current can be kept within the whole strain range (insert in Fig.4(b)). And the higher E-field will weaken this spin-polarization for all cases with different strains

DOI:10.1063/1674-0068/28/cjcp1505087 ©2015 Chinese Physical Society

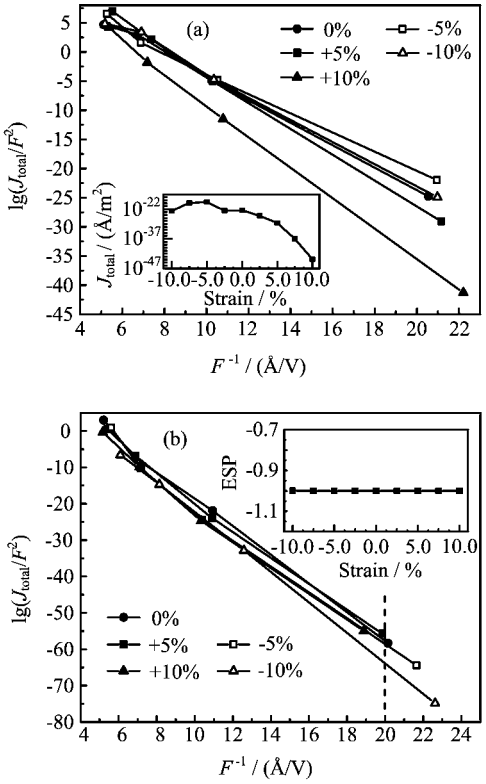

FIG. 4 The FN plots of the field emission from two types of ribbons under different uniaxial strains. (a) The ZGNR-CE (inset: the total emission current density $J_{\rm total}$ as a function of the uniaxial strain under the nominal E-field of 0.05 V/Å). (b) The ZGNR-AE (inset: the ESP of its emission current as a function of the uniaxial strain under the nominal E-field of 0.05 V/Å).

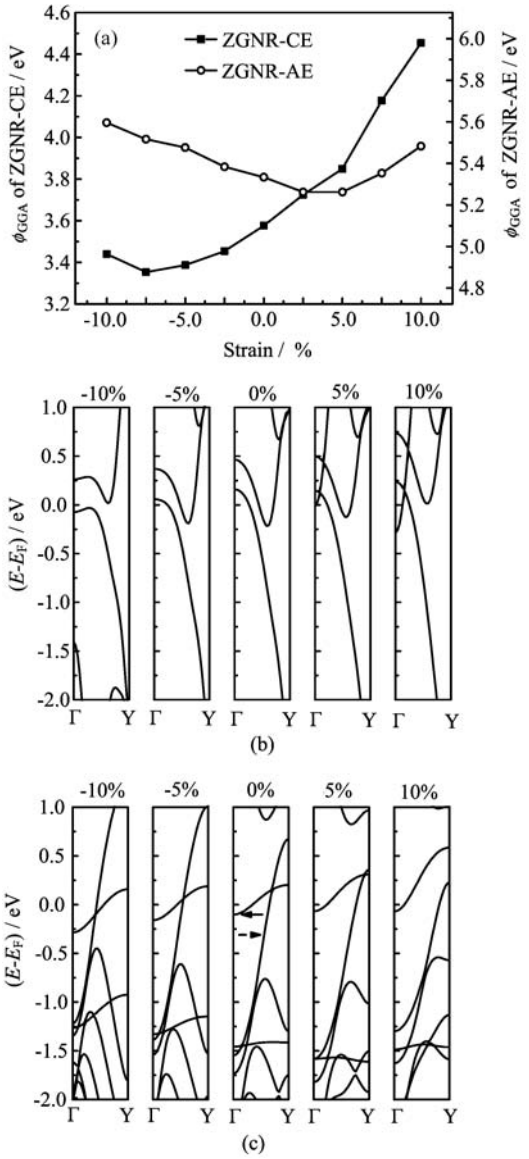

FIG. 5 (a) The work functions of two types of ribbons as functions of the uniaxial strain. The band structures of (b) ZGNR-CE and (c) ZGNR-AE under different uniaxial strains.

(not shown), similar to the case without strain as described before.

In order to reveal mechanisms of the strain-dependences of the emission currents of two types of ribbons under the lower E-field, their work functions and band structures under different strains are presented in Fig.5. For the ZGNR-CE, it is found that strain-dependence of its work function is just opposite to that of its emission current (see Fig.5(a) and insert in Fig.4(a)), which is reasonable since increase (decrease) of the work function will weaken (enhance) the emission current as shown by the FN formula. So this especial strain-dependence of the work function determines the modulation of the emission current by the strain. We can interpret this dependence as follows: both the increase of tensile strain and decrease of compressive strain mean increase of the area A per primitive cell in the xy-plane; therefore, according to Eq.(4), the work function of the ZGNR-CE will also increase when the tensile strain increases or compressive strain decreases, since it has positive edge dipole moment as discussed before; an abnormal increase of its work function when the compressive strain is larger than about -5% may be related to a metal-semiconductor transition, which opens a small energy gap under the compressive strain of -10% as shown by Fig.5(b) and then influences applicability of the edge dipole model in interpreting the work function. For the ZGNR-AE, the strain-dependence of its work function (Fig.5(a)) has also similar relationship with that of its emission current indicated by dash line in Fig.4(b). When the strain is smaller than 5%, its work function always decreases with the increase of tensile strain and decrease of compressive strain, which results from its negative net edge dipole moment due to the dangling bond states according to the above discussion about the ZGNR-CE. Its

DOI:10.1063/1674-0068/28/cjcp1505087 ©2015 Chinese Physical Society

work function has also an abnormal increase when the tensile strain is larger than about 5%, and decrease of electron population of the dangling bond states (indicated by solid arrow in Fig.5(c), and bringing negative edge dipole moment) and increase of electron population of the π-conjugated edge states (indicated by dash arrow in Fig.5(c), and bringing positive edge dipole moment) along with their induced variation of the net edge dipole moment should be responsible for it. The domination of the dangling bond states near the $E_{\rm F}$ and Γ point for different strains (Fig.5(c)) also ensures that under the lower E-field its high spin-polarization can survive the varied strain.

IV. CONCLUSION

We have applied a first-principles method to study the field emission from the two types of ZGNR terminated with C-O-C ether groups. The energy distribution and the intensity of their emission current under different E-fields are simulated. It is revealed that the comparatively lower work function of the ZGNR-CE makes that it can produce stronger field emission current than the ZGNR without ether groups, and the field emission of the ZGNR-AE has very high spin-polarization. Under the lower E-field, the effect of the uniaxial strain on the emission current is obvious for two types of ribbons, but the ESP of the ZGNR-AE keeps unchanged against the varied strain. These phenomena can be understood by analyzing their band structure and work function jointly with the edge dipole model.

V. ACKNOWLEDGMENTS

This work was supported by the National Key Basic Research Program (No.2011CB921404), the National Natural Science Foundation of China (No.21273210), Chinese Academy of Sciences (No.XDB01020300), the Fundamental Research Funds for the Central Universities, and USTCSCC.

[1] R. H. Baughman, A. A. Zakhidov, and W. A. de Heer, Science **297**, 787 (2002).
[2] S. Han and J. Ihm, Phys. Rev. B **61**, 9986 (2000).
[3] M. Araidai, Y. Nakamura, and K. Watanabe, Phys. Rev. B **70**, 245410 (2004).
[4] R. H. Fowler and L. Nordheim, Proc. R. Soc. London, Ser. A **119**, 173 (1928).
[5] C. D. Ehrlich and E. W. Plummer, Phys. Rev. B **18**, 3767 (1978).
[6] C. Adessi and M. Devel, Phys. Rev. B **62**, 13314 (2000).
[7] Y. Gohda, Y. Nakamura, K. Watanabe, and S. Watanabe, Phys. Rev. Lett. **85**, 1750 (2000).
[8] K. Tada and K. Watanabe, Phys. Rev. Lett. **88**, 127601 (2002).
[9] S. Dutta and S. K. Pati, Carbon **48**, 4409 (2010).
[10] S. F. Huang, T. C. Leung, B. Li, and C. T. Chan, Phys. Rev. B **72**, 035449 (2005).
[11] C. F. Shih, K. S. Liu, and I. N. Lin, Diam. Relat. Mater. **9**, 1591 (2000).
[12] N. Park, S. W. Han, and J. Ihm, Phys. Rev. B **64**, 125401 (2001).
[13] W. T. Zheng, C. Q. Sun, and B. K. Tay, Solid State Commun. **128**, 381 (2003).
[14] J. Xu, J. Mei, X. H. Huang, X. Li, Z. Li, W. Li, and K. Chen, Appl. Phys. A **80**, 123 (2005).
[15] W. Wang and Z. Li, Appl. Phys. A **109**, 353 (2012).
[16] H. Yamaguchi, K. Murakami, G. Eda, T. Fujita, P. Guan, W. Wang, C. Gong, J. Boisse, S. Miller, M. Acik, K. Cho, Y. J. Chabal, M. Chen, F. Wakaya, M. Takai, and M. Chhowalla, ACS Nano **5**, 4945 (2011).
[17] W. Wang, J. Shao, and Z. Li, Chem. Phys. Lett. **522**, 83 (2012).
[18] B. Li, T. C. Leung, and C. T. Chan, Phys. Rev. Lett. **97**, 087201 (2008).
[19] P. Koskinen, S. Malola, and H. Häkkinen, Phys. Rev. Lett. **101**, 115502 (2008).
[20] G. Kresse and J. Hafner, Phys. Rev. B **47**, 558 (1993).
[21] G. Kresse and J. Hafner, Phys. Rev. B **49**, 14251 (1994).
[22] G. Kresse and J. Furthmuller, Phys. Rev. B **54**, 11169 (1996).
[23] G. Kresse and J. Furthmuller, Comp. Mater. Sci. **6**, 15 (1996).
[24] G. Kresse and J. Joubert, Phys. Rev. B **59**, 1758 (1999).
[25] J. P. Perdew, K. Burke, and M. Ernzerhof, Phys. Rev. Lett. **77**, 3865 (1996).
[26] H. Lee, Y. W. Son, N. Park, S. Han, and J. Yu, Phys. Rev. B **72**, 174431 (2005).
[27] E. Wigner and J. Bardeen, Phys. Rev. **48**, 84 (1935).
[28] X. Peng, F. Tang, and A. Copple, J. Phys.: Condens. Matter **24**, 075501 (2012).

DOI:10.1063/1674-0068/28/cjcp1505087 ©2015 Chinese Physical Society